



issn: 1600-5767 journals.iucr.org/j

Symmetry-mode analysis for local structure investigations using pair distribution function data

Parker K. Hamilton, Jaime M. Moya, Alannah M. Hallas, E. Morosan, Raju Baral and Benjamin A. Frandsen

J. Appl. Cryst. (2023). **56**, 1192–1199



Author(s) of this article may load this reprint on their own web site or institutional repository and on not-for-profit repositories in their subject area provided that this cover page is retained and a permanent link is given from your posting to the final article on the IUCr website.

For further information see https://journals.iucr.org/services/authorrights.html

research papers



ISSN 1600-5767

Received 22 March 2023 Accepted 2 July 2023

Edited by A. H. Liu, HPSTAR and Harbin Institute of Technology, People's Republic of China

Keywords: total scattering; pair distribution function; symmetry modes; local structure; local symmetry breaking.

Supporting information: this article has supporting information at journals.iucr.org/j

Symmetry-mode analysis for local structure investigations using pair distribution function data

Parker K. Hamilton,^a Jaime M. Moya,^{b,c} Alannah M. Hallas,^{d,e} E. Morosan,^{c,f} Raju Baral^a and Benjamin A. Frandsen^a*

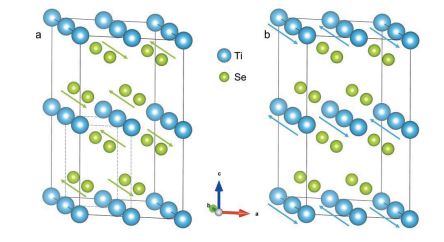
^aDepartment of Physics and Astronomy, Brigham Young University, Provo, UT 84602, USA, ^bApplied Physics Program, Rice University, Houston, TX 77005, USA, ^cDepartment of Physics and Astronomy, Rice University, Houston, TX 77005, USA, ^dQuantum Matter Institute, University of British Columbia, Vancouver, BC, V6T 1Z4, Canada, ^eDepartment of Physics and Astronomy, University of British Columbia, Vancouver, BC, V6T 1Z1, Canada, and ^fRice Center for Quantum Materials, Rice University, Houston, TX 77005, USA. *Correspondence e-mail: benfrandsen@byu.edu

Symmetry-adapted distortion modes provide a natural way of describing distorted structures derived from higher-symmetry parent phases. Structural refinements using symmetry-mode amplitudes as fit variables have been used for at least ten years in Rietveld refinements of the average crystal structure from diffraction data; more recently, this approach has also been used for investigations of the local structure using real-space pair distribution function (PDF) data. Here, the value of performing symmetry-mode fits to PDF data is further demonstrated through the successful application of this method to two topical materials: TiSe2, where a subtle but long-range structural distortion driven by the formation of a charge-density wave is detected, and MnTe, where a large but highly localized structural distortion is characterized in terms of symmetry-lowering displacements of the Te atoms. The analysis is performed using fully open-source code within the DiffPy framework via two packages developed for this work: isopydistort, which provides a scriptable interface to the ISODISTORT web application for group theoretical calculations, and isopytools, which converts the ISODISTORT output into a DiffPy-compatible format for subsequent fitting and analysis. These developments expand the potential impact of symmetry-adapted PDF analysis by enabling highthroughput analysis and removing the need for any commercial software.

1. Introduction

Total scattering techniques are a powerful tool for understanding the structure of solids (Billinge & Kanatzidis, 2004; Keen, 2020). These methods include in the analysis not only the Bragg scattering that arises from the long-range correlations of the average structure but also the diffuse scattering that originates from short-range correlations deviating from the average structure. The use of total scattering therefore gives a window into short-range structural correlations that are missed by Bragg peak analysis and other probes of the average structure.

Pair distribution function (PDF) analysis is a well established analytic technique for total scattering data that involves Fourier transformation of the total scattering pattern to yield a map of the interatomic distances as a function of real-space distance r (Egami & Billinge, 2012). The scattering arising from correlated distortions of the local structure is thereby recast from broad diffuse signals in reciprocal space to sharper more localized signals in real space. This can lend a more intuitive interpretive power to the real-space PDF data and also allow for more effective modeling of the local structure (Billinge & Levin, 2007).



A typical objective of PDF analysis is to identify and characterize symmetry-breaking distortions in the local structure that average to zero over longer length scales. Local symmetry breaking of this type can provide crucial information about the underlying physics of the material under investigation (Billinge & Kanatzidis, 2004; Billinge & Levin, 2007; Young & Goodwin, 2011; Keen & Goodwin, 2015; Dagotto, 2005; Tokura et al., 2017; Desgranges et al., 2018; Zhu et al., 2021). In the commonly used 'small-box modeling' or 'real-space Rietveld' approach, one often starts with a structural model appropriate for the average structure, fits the model to the low-r portion of the data, and looks for systematic misfits that provide evidence for and information about any short-range structural distortions. The next step is then typically to test lower-symmetry models against the data to see if the fit improves, and if so, attempt to determine what physical insights can be gained from the lower-symmetry model (Chepkemboi et al., 2022).

Two commonly occurring obstacles can make this strategy difficult. First, selecting candidate lower-symmetry models can often be an *ad hoc* process requiring tedious guesswork by the PDF analyst, and even if some distorted model that improves the fit is identified, it may not be clear whether other distorted models could provide equally good or even better fits. In some cases, theoretical inputs or experimental data from other probes such as high-resolution diffraction or Raman spectroscopy (Forse *et al.*, 2015) may help guide the choice of distorted model, but such inputs are not always available. Second, lower-symmetry models will naturally have a greater number of free parameters [*e.g.* atomic positions and atomic displacement parameters (ADPs)] to be optimized in the fit, which can impede the optimization routine from converging reliably.

These difficulties apply to both PDF and Rietveld analysis of diffraction data. A promising way of overcoming these challenges is to use a symmetry-adapted fitting scheme using the tools of group theory, as has been demonstrated for Rietveld refinements with diffraction data (Kerman et al., 2012; Gawryluk et al., 2019). Using software such as ISODISTORT (Campbell et al., 2006; Stokes et al., 2023), one can start with a parent structure and systematically explore distorted child structures down to arbitrarily low symmetry and up to an arbitrarily large supercell. Comparing the fit results allows one to build a more complete picture of potential distorted structures that could explain the data. This addresses the first of the previously mentioned challenges. In addition, one can define as fit variables the amplitudes of the symmetry modes allowed for a given structure, in place of the atomic coordinates for individual atoms that are conventionally used as fit variables. A single variable in the form of a mode amplitude may therefore control the collective motion of several distinct atoms. Because structural distortions often correspond to a small number of symmetry modes taking nonzero amplitudes (Kerman et al., 2012), the use of symmetrymode amplitudes as a basis for the fit variables can greatly reduce the number of variables required to achieve a good fit, leading to more robust convergence. In addition, the symmetry modes relevant for a given structural distortion can be identified directly from the fit, providing greater clarity to the physical interpretation of the fit results. This feature of a symmetry-adapted fitting scheme addresses the second of the challenges mentioned previously.

Recently, symmetry-mode analysis has also been applied to PDF data (Bird et al., 2021a). Bird and co-workers introduced a procedure for refining distortion-mode amplitudes from PDF data that entails (i) downloading the symmetry-mode information from the ISODISTORT web application, (ii) running a script to convert the output into a format that can be read by the commercial structural refinement software TOPAS-Academic (Coelho, 2018), and (iii) iterating through a series of refinements in TOPAS to identify and evaluate candidate distortion modes. The approach was successfully used to characterize dynamic distortions in the negative thermal expansion material ScF₃ and short-range distortions in the prototypical ferroelectric BaTiO₃, demonstrating that a symmetry-adapted fitting scheme can be applied to PDF analysis, providing the aforementioned advantages over conventional fitting methods. It has since been applied to ReO₃ (Bird et al., 2021b) and BaTiO₃ under pressure (Herlihy et al., 2022), suggesting that this approach is widely applicable.

Here, we further demonstrate the value of symmetryadapted PDF analysis and introduce alternative software tools for implementing this approach in an automatable and fully open-source way. We have developed the open-source Python packages isopydistort and isopytools, which, respectively, enable automatic calls to ISODISTORT from a Python script and convert the ISODISTORT output into a format suitable for structural refinements using the open-source DiffPy library (Juhás et al., 2015). This work broadens the impact of symmetry-adapted PDF analysis by eliminating exclusive reliance on commercial software and making high-throughput analysis possible. We use this method to study two complementary examples drawn from materials of significant recent interest: the charge-density-wave (CDW) compound TiSe2, which displays a long-range but subtle structural distortion, and the high-performance thermoelectric candidate MnTe, where we observe a large but highly localized distortion. In both cases, we identify the relevant distortions and achieve excellent PDF fits through a systematic and automated exploration of all possible symmetry modes. The results further emphasize the advantages of using symmetry modes when performing structural refinements and suggest that the open-source tools introduced here can be successfully applied to a wide variety of materials.

2. Methodology: refining distortion models using symmetry modes

A distortion removes certain symmetry elements of the parent space group. The remaining symmetry elements that persist in the distorted structure constitute the 'distortion symmetry' or 'isotropy subgroup' and form the space group of the distorted structure. In this work, we consider only displacive distortions involving changes in the positions of the atoms. To test

distorted structural models against PDF data, we use ISODISTORT, which can generate all possible distortion symmetries of a given parent structure for a user-specified supercell and space-group type. Furthermore, ISODISTORT can express the distortion models using either the traditional xyz basis of atomic coordinates or the symmetry-informed basis of symmetry-mode amplitudes, which are constructed from the basis vectors of the irreducible representation (irrep) associated with the given distortion. These two bases – the xyz basis and the mode-amplitude basis – are related by a linear transformation calculated by ISODISTORT. In general, a single mode amplitude can affect the positions of multiple atoms, and the displacement of a single atom may be determined by the amplitudes of multiple modes. Since both bases describe the same distortion space, the number of symmetry modes always equals the number of independent atomic coordinates. For P1 symmetry, there are no constraints on atomic positions, so for a supercell with N atoms, there are 3Natomic coordinates and 3N symmetry modes. For higher symmetries, of course, there will be fewer degrees of freedom, since not all atomic displacements will be independent. An example of a symmetry mode from the TiSe2 study described later is shown in Fig. 1.

The traditional approach to refining a distorted structural model is to use the *xyz* basis as fit variables and refine the positions of the atoms directly. However, if the correct distortion symmetry is not known (and sometimes even if it is), there may be so many degrees of freedom that standard fitting algorithms have difficulty converging to a good result. Recognizing that distortions are often dominated by one or a few modes while the others remain inactive, it can be much more effective to use mode amplitudes as fit variables rather than atomic coordinates (Kerman *et al.*, 2012). A small number of free parameters corresponding to the mode amplitudes can therefore capture collective displacements of multiple atoms that would otherwise require a larger number of atomic coordinates to describe. Furthermore, the fitting scheme can be organized such that one symmetry mode is

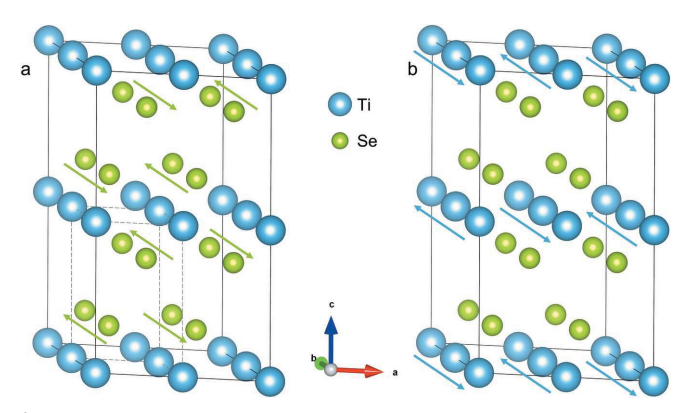


Figure 1 A $2 \times 2 \times 2$ supercell of the $P\overline{3}m1$ structure of TiSe₂, visualized using *VESTA* (Momma & Izumi, 2011). The arrows depict distortions belonging to the L_1^- irrep. (a) The Se distortion corresponding to the E(c) mode. The dashed lines indicate the parent cell. (b) The Ti distortion corresponding to the $E_u(c)$ mode.

tested at a time while all the others remain fixed, which allows the identification of relevant modes much more effectively than would be possible by cycling through the individual atomic coordinates. Finally, this symmetry-informed approach directly reveals which symmetry modes are active in a given structure, yielding insight into the underlying physics at play in the material.

In this work, we use the original open-source Python packages *isopydistort*, which interfaces directly with the *ISODISTORT* server online through a Python script inspired by similar functionality available in *GSAS-II* (Toby & Von Dreele, 2013), and *isopytools*, which converts the *ISO-DISTORT* output into a format compatible with the open-source *DiffPy* suite for PDF fitting and analysis. These developments remove the need to click through the *ISODISTORT* web tool to generate the distortion models, providing a significantly greater degree of automation and flexibility when performing symmetry-mode fits to PDF data, all within a fully open-source software environment. Below we describe the typical workflow, which can be carried out completely within a Python script or *Jupyter* notebook using the functions defined in our Python packages.

- (i) Upload a crystallographic information file (CIF) corresponding to the parent structure (e.g. as determined by Rietveld refinements to diffraction data or by PDF fits conducted over a long fitting range) to the ISODISTORT server, together with an optional dictionary of ISODISTORT arguments such as the lattice basis of the supercell relative to the parent cell or the desired space group of the child structure (P1 by default). This is done with the isopydistort package. The code interfacing with ISODISTORT then automatically works through the steps to produce a human-readable file (in TOPAS format) containing all the symmetry modes compatible with the specified supercell and space group. This file is automatically downloaded from the ISODISTORT server. Other ISODISTORT output files can also be requested by the user, such as a CIF or interactive distortion visualization file.
- (ii) Create a *DiffPy*-compatible structure object from the *ISODISTORT* output using the *isopytools* package.
- (iii) Input the symmetry-mode amplitudes as variables to be optimized in the fit, together with the usual fit variables such as a scale parameter, lattice parameters and ADPs. The *isopytools* package automatically implements the appropriate constraints relating the mode amplitudes to the atomic coordinates based on the *ISODISTORT* output.
- (iv) Use diffpy.srfit to carry out the fit however the user desires. For example, the user can cycle through each mode amplitude individually, refine multiple amplitudes in arbitrarily defined groups, perform multiple fits with random starting values, impose a cost for activating additional modes (Kerman et al., 2012), establish a threshold for improvement in the fit quality to consider a mode active (Bird et al., 2021a) etc.
- (v) Modify the diffpy.srfit script as desired for automatic batch fits to multiple data sets, different fitting ranges etc.

We followed this basic workflow to study the distortions present in TiSe₂ and MnTe.

3. Experimental details

A powder sample of TiSe₂ was synthesized via solid-state reaction. Powdered Ti and Se were weighed out in the atomic ratio of Ti:Se 1:2.02 and ground together in accordance with the work of Moya *et al.* (2019). The resultant powder was sealed in a quartz tube under \sim 3 Torr (1 Torr = 133.322 Pa) of partial argon atmosphere and heated at a rate of 323 K h⁻¹ to 923 K. The sample remained at 923 K for 48 h before being quenched to ambient temperature.

The powder sample of MnTe was the same one as used by Baral *et al.* (2022). It was prepared by thoroughly mixing stoichiometric amounts of Mn powder and Te pieces in an argon glove box, sealing the mixture in an evacuated quartz tube and placing it in a furnace at 1223 K for 6 h. The ampoule was then quenched in iced water and annealed further at 923 K for 72 h. A mortar and pestle were used to grind the sample into a fine powder in the glove box.

The X-ray total scattering experiments were performed at the National Synchrotron Light Source II (NSLS-II) at Brookhaven National Laboratory (USA) on beamline 28-ID-1. The incident wavelength was 0.167 Å. Finely ground powder samples were loaded into thin Kapton capillaries sealed with clay. The capillaries were loaded into a liquidhelium cryostat mounted on the beamline, allowing for continuous temperature control between 5 and 500 K, although the maximum temperature achieved in the present study was 300 K. A large amorphous silicon area detector was used to record the diffraction patterns, which were azimuthally integrated using DIOPTAS (Prescher & Prakapenka, 2015). The integration was performed using 4096 radial points and 360 azimuthal points. The resulting one-dimensional diffraction patterns were normalized and Fourier transformed with $Q_{\text{max}} = 25 \,\text{Å}^{-1}$ to produce the PDF using the xPDFsuite program (Yang et al., 2015).

The neutron total scattering experiments were performed on the Nanoscale-Ordered Material Diffractometer (NOMAD) at the Spallation Neutron Source of Oak Ridge National Laboratory (USA) (Neuefeind *et al.*, 2012). The powder samples were loaded into quartz capillaries and mounted in the beam. Neutron scattering data were collected for an integrated proton current of 4 C and then reduced and transformed with $Q_{\rm max} = 25~{\rm \AA}^{-1}$ using *ADDIE* (McDonnell *et al.*, 2017), the automatic data reduction program on NOMAD.

4. Results

4.1. TiSe₂

The transition metal dichalcogenide TiSe_2 is interesting for its complex electronic properties (Manzeli et al., 2017; Yin et al., 2021), particularly the formation of a CDW state below $\sim 200~\mathrm{K}$ (Di Salvo et al., 1976). A subtle structural distortion accompanies the CDW transition, making TiSe_2 a good test case for the ability to pick out small but long-range distortions in PDF data. This will be complementary to the MnTe test case, where the distortion is large but highly localized.

The CDW state in TiSe₂ forms a $2 \times 2 \times 2$ superlattice of the $P\overline{3}m1$ high-temperature parent structure (Di Salvo *et al.*, 1976). The supercell contains 24 atoms (eight formula units) and therefore a total of 72 degrees of freedom for P1 symmetry, which we selected to provide the most general possible exploration of potential distortions. For each of the 72 symmetry modes, we performed a PDF fit to the 5 K data from 1.5 to 20 Å by first optimizing the lattice parameters and scale factor, then adding the symmetry-lowering mode amplitude and the displacement allowed in the parent space group $(P\overline{3}m1)$, and finally adding the ADPs. To quantify the impact of each symmetry mode, we use the goodness-of-fit metric

$$R_{\rm w} = \left\{ \frac{\sum_{i} \left[G_{\rm obs}(r_i) - G_{\rm calc}(r_i) \right]^2}{\sum_{i} G_{\rm obs}^2(r_i)} \right\}^{1/2},\tag{1}$$

where r_i is the *i*th value in the *r* grid of the experimental data, $G_{\rm obs}$ is the observed PDF and $G_{\rm calc}$ is the calculated PDF. A lower value of $R_{\rm w}$ indicates better agreement with the data. In Fig. 2(a) we plot $R_{\rm w}$ versus mode amplitude for all 72 modes tested individually, along with a horizontal line at $R_{\rm w}=0.0571$ marking the base value with no symmetry-breaking modes included.

We see that most of the modes provide minimal improvement to the fit. However, two groups of modes improve the fit significantly more than the others, indicated by the arrows on the figure. These are the Ti E_u and the Se E modes of the $L_1^$ irrep, corresponding to in-plane distortions of the Ti and Se atoms (refer to Fig. 1). Each group of modes includes three equivalent distortions that are rotated 120° from each other and, given the 1D nature of the PDF data, have identical effects on the calculated PDF. The L_1^- irrep to which these modes belong is precisely the one responsible for the known CDW distortion in TiSe2, which consists of equal superpositions of the three branches of the Ti E_u and the Se Emodes (Subedi, 2022). That the PDF fits naturally pick out these modes validates the use of this approach for TiSe₂ and confirms the ability of this symmetry-motivated fitting strategy to identify even rather subtle distortions. These same modes likewise provided the most improvement by a wide margin for longer-ranged fits up to 50 Å. The fit was improved further when the same branches of the Ti and Se modes were refined together [e.g. $E_u(a)$ and E(a) for Ti and Se, respectively], lowering $R_{\rm w}$ from 0.0571 to 0.0542 for the 1.5–20 Å X-ray fits. This difference is shown to be statistically significant in the supporting information. The corresponding fit is displayed in Fig. 2(c). A portion of the fit residual is also shown in Fig. 2(c), together with the fit residual corresponding to the undistorted structure for comparison. Although the difference is subtle, the distorted model is seen to reduce the fit residual systematically, except for a few distinct points. The refined mode amplitudes at 5 K equate to displacements of 0.047 (3) and 0.024 (4) Å for Ti and Se, respectively, with the Ti-Se nearest-neighbor distance decreasing by approximately 0.05 Å. These values are close to the previously published results using traditional neutron and X-ray diffraction (Di Salvo et al., 1976; Fang et al., 2017).

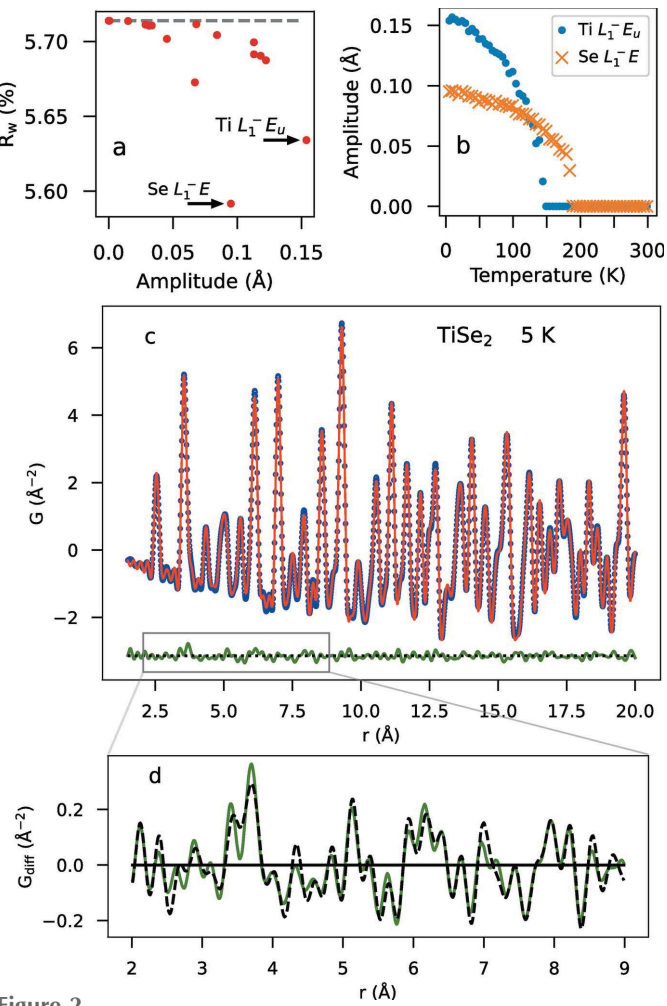


Figure 2 (a) A plot of $R_{\rm w}$ versus mode amplitude for the 72 distortion modes. The arrows indicate the modes that improved the fit most significantly, namely the Ti $E_{\rm u}$ and Se E modes of the $L_{\rm l}^{-}$ irrep. Note that 72 distinct points are not visible, because multiple modes may have the same effect on the calculated powder PDF pattern and therefore overlap on the plot. (b) The temperature dependence of the refined amplitudes of the Ti $E_{\rm u}(a)$ and Se E(a) modes of the $L_{\rm l}^{-}$ irrep. (c) A representative PDF fit to data at 5.1 K with both modes active. The blue symbols represent the experimental data, the red curve the calculated PDF and the green curve the fit residual, offset for clarity. (d) A comparison of a portion of the fit residual using the distorted model (green curve) and the undistorted parent model (dashed black curve).

Having identified the active distortion modes at 5 K, we then performed fits to the remaining X-ray PDF data sets with the Ti $E_u(a)$ and Se E(a) modes included individually to examine the temperature dependence of the distortion. As illustrated in Fig. 2(b), we see that the mode amplitudes decrease with increasing temperature until they reach zero between approximately 150 and 200 K, corresponding reasonably well to the accepted CDW transition temperature of around 200 K (Di Salvo *et al.*, 1976). The discrepancy in temperature may be due to the difficulty in resolving very small displacements near the transition in our data; this is consistent with the fact that the reduction in R_w and the mode amplitude become non-zero at the same temperature (not shown in the figure). The figure demonstrates how the mode

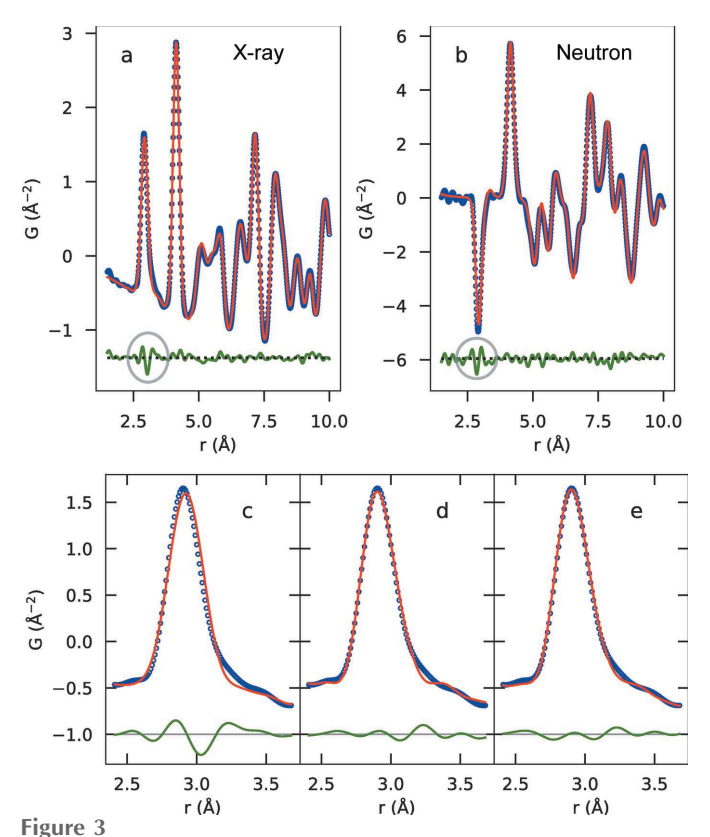
amplitudes serve as order parameters to identify structural transitions. Interestingly, the refined Se E(a) mode amplitude becomes non-zero below 190 K, while the Ti $E_u(a)$ mode amplitude does so only below about 145 K. This may indicate that the Se distortion drives the CDW transition, but it may also occur simply because the weaker scattering strength of Ti reduces the sensitivity of the fits to Ti displacements compared with Se displacements. Additional studies could provide further clarity on this. Finally, we compare these results with fits performed to neutron PDF data collected at 100 and 300 K. The fits at 100 K yielded mode amplitudes of 0.18 (3) and 0.08 (2) Å for the Ti $E_u(a)$ and Se E(a) modes, respectively. The corresponding values determined from the X-ray fits are 0.12 (1) and 0.08 (1) \mathring{A} . At 300 K, the mode amplitudes refined to values below 0.0002 Å, which is not meaningfully different from zero. This is expected in the undistorted state above the CDW transition.

4.2. MnTe

Hexagonal MnTe (space group P63/mmc) is an antiferromagnetic semiconductor that has garnered interest as a potential high-performance thermoelectric material (Xu et al., 2017; Ren et al., 2017; Dong et al., 2018; Zheng et al., 2019; Baral et al., 2022) and as a platform for antiferromagnetic spintronics (Kriegner et al., 2016). In the context of the present work, MnTe is a useful example because PDF analysis reveals a large short-range distortion of the local structure that exists at room temperature. This is manifest as a significant misfit below approximately 3.5 Å in the PDF fits when the published hexagonal structure is used (D'Sa et al., 2005), as shown by the circled portions of the fit residuals in Figs. 3(a) and 3(b) for X-ray and neutron PDFs, respectively. The data were collected at 300 K. An enlarged view of the misfit for the X-ray PDF pattern is shown in Fig. 3(c), revealing that the calculated peak is off-centered relative to the observed peak. The origin and significance of this feature in the local structure will be discussed elsewhere, but the objective here is to demonstrate that a symmetry-driven approach can be successfully applied to highly localized structural distortions, in addition to longrange distortions such as the example given by TiSe₂.

To investigate the local distortion in MnTe, we systematically tested each of the 12 displacive symmetry modes in the conventional unit cell assuming P1 symmetry. We restricted the fit range to 1.5–3.75 Å, since the misfit is localized to the first large peak in the PDF pattern. To avoid over-fitting to this short data range, we fixed the lattice parameters to the values determined from a longer-range fit (1.5–20 Å) and optimized only a scale factor, an isotropic displacement parameter for each atomic species and the symmetry-mode amplitude. The peak-sharpening parameter δ_1 was fixed to the value determined from the longer-range fit.

Of the 12 symmetry mode amplitudes, 11 had only a small effect on the fit when tested individually. However, the Te E'(a) mode of the Γ_5^+ irrep improved the fit dramatically, reducing $R_{\rm w}$ from 0.115 to 0.058 for the X-ray fit and from 0.106 to 0.058 for the neutron fit. A plot of $R_{\rm w}$ versus mode amplitude is shown in the supporting information. Both the



(a) An X-ray PDF fit to MnTe at 300 K using the published hexagonal structure (D'Sa et al., 2005). The blue symbols and red curve show the observed and calculated PDFs, respectively, while the green curve shows the fit residual (offset vertically for clarity). (b) The same as panel (a) but for neutron PDF data [with the magnetic PDF (Frandsen et al., 2014; Frandsen & Billinge, 2015) included in the fit]. (c) An enlarged view of the X-ray PDF fit in panel (a), highlighting the failure of the model for the first peak. (d) The fit when the Te E'(a) mode of the Γ_5^+ irrep is active. (e) The fit when the Te E'(a) mode of the Γ_5^+ irrep and the Mn $E_u(a)$ mode of the Γ_6^- irrep are active.

neutron and X-ray data sets yielded a mode amplitude corresponding to a Te displacement of \sim 0.126 (4) Å. The improved fit is shown for the X-ray data in Fig. 3(d); notably, the calculated peak is now centered on the experimental peak. Equivalent plots for the neutron PDF analysis are shown in the supporting information. The Te E'(a) mode of the Γ_5^+ irrep corresponds to antiparallel displacements of the two Te atoms toward the nearest face of the unit cell, as illustrated in Fig. 4. If this were a coherent distortion throughout the entire crystal structure, the crystallographic symmetry would be lowered to space group Cmcm.

Refining pairs of symmetry-mode amplitudes simultaneously improves the fit slightly. Fig. 3(e), for example, shows the X-ray fit when the same Te E'(a) mode of the Γ_5^+ irrep and the Mn $E_u(a)$ mode of the Γ_6^- irrep are both active. The refined amplitudes were 0.09 Å for Γ_5^+ and -0.17 Å for Γ_6^- , and the value of $R_{\rm w}$ was 0.038. However, other pairs of modes yielded equally good fits, indicating that the data range over which the local distortion is observed is insufficient to remove all ambiguity. Whether or not the peak-sharpening parameters δ_1 or δ_2 were included also influenced which mode pairs yielded the best fit. On the other hand, the single-mode refinements

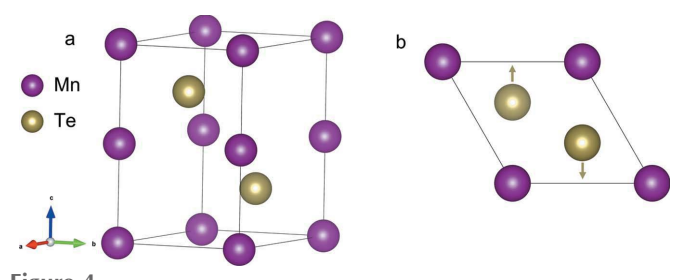


Figure 4 (a) The conventional unit cell of MnTe, visualized with VESTA (Momma & Izumi, 2011). (b) A view of the unit cell looking down the c axis, with the Te displacements of the $\Gamma_5^+E'(a)$ shown by the arrows.

were robust against variations in the choice of δ_1 or δ_2 (or no peak-sharpening function at all), the number of unique ADPs, and the starting values of the variables, building confidence in the reliability of the single-mode results. Finally, we note that symmetry-mode fits performed against a data range exceeding \sim 5 Å were unable to fit the low-r and high-r peaks simultaneously; instead, the fits yielded negligibly small mode amplitudes such that the longer-range peaks were well described at the expense of the first large peak. This indicates that the distortion in MnTe is highly localized.

5. Discussion and conclusion

We have demonstrated the utility of the symmetry-mode approach to fitting PDF data for two complementary use cases. In the case of TiSe2, we identified a structural phase transition present over the full r range of the data in a more straightforward manner than would have been possible using traditional PDF fitting methods with xyz atomic coordinates as fit variables. The amplitudes of the active symmetry modes served as structural order parameters to show subtle but observable changes to the long-range structure, consistent with the published results. Here, the advantage of the symmetry-driven methods over the traditional xyz approach is the reduced number of free parameters necessary to test and identify distorted structural models that fit the data. Only two non-zero mode amplitudes were necessary to characterize the distorted structure, while systematic testing of the individual atomic coordinates would have required a much larger number of fit variables to arrive at the same result.

The MnTe case also offers a proof of concept for fitting distortions with shorter correlation lengths. The distortion was only apparent in the data below about 4 Å. The flexibility of our implementation allows for the isolation, or concurrent testing, of individual modes and groups of modes as defined by the user. For MnTe, we identified a single Te mode that resulted in a much better fit when activated. The extremely localized nature of this distortion obscures the notion of symmetry modes somewhat, but the symmetry-mode basis nevertheless provided a useful parameterization, leading us to identify an in-plane distortion of the Te atoms as the likely cause of the misfit in the original fit.

A benefit of using the flexible *DiffPy* fitting framework is that users can customize the fitting procedure in any way they

desire. For example, one could easily execute the fit multiple times with random starting values, impose a penalty to the cost function for each active symmetry mode, or set a threshold improvement value in $R_{\rm w}$ to allow a mode to be considered active. These strategies have all been suggested previously as ways of improving the reliability of exhaustive symmetry-mode testing (Bird et al., 2021a; Kerman et al., 2012). Our code can also be extended in a straightforward manner to include the rotational, occupational and magnetic modes calculated by ISODISTORT, although that is beyond the scope of the present work.

The study of molecular materials can also benefit from symmetry-mode analysis if the molecules contain rigid units (Liu *et al.*, 2018).

We expect that symmetry-adapted PDF analysis will become increasingly common in the field of total scattering, leading to new physical insights into the local structure of materials.

6. Code availability and usage

The analysis methods introduced in this work are based on fully open-source software. We have developed two new packages as part of this work: *isopydistort* (https://github.com/FrandsenGroup/isopydistort) for automated interactions with the *ISODISTORT* web-based software, and *isopytools* (https://github.com/FrandsenGroup/isopytools) for adapting the *ISODISTORT* output to be compatible with the *DiffPy* library (Juhás *et al.*, 2015). Example scripts and data files corresponding to the analysis presented in this work are also available in the supporting information.

Acknowledgements

We thank Branton Campbell for valuable discussions regarding symmetry-adapted distortion modes and *ISO-DISTORT*. We acknowledge Brian Toby and Robert von Dreele, who developed the first Python code to interface with *ISODISTORT* as part of their *GSAS-II* program.

Funding information

Work by P. K. Hamilton, R. Baral and B. A. Frandsen was supported by the US Department of Energy, Office of Science, Office of Basic Energy Sciences (DOE-BES) through award No. DE-SC0021134. A. M. Hallas acknowledges support from the Natural Sciences and Engineering Research Council of Canada (NSERC) and the CIFAR Azrieli Global Scholars program. J. M. Moya and E. Morosan acknowledge partial support from the National Science Foundation Division of Materials Research grant No. 1903741 and the Robert A. Welch Foundation grant C-2114. This study used resources at the Spallation Neutron Source (SNS), a DOE Office of Science User Facility operated by Oak Ridge National Laboratory. This research used beamline 28-ID-1 of the National Synchrotron Light Source II, a US Department of Energy (DOE) Office of Science User Facility operated for the

DOE Office of Science by Brookhaven National Laboratory under contract No. DE-SC0012704.

References

Baral, R., Christensen, J., Hamilton, P., Ye, F., Chesnel, K., Sparks, T. D., Ward, R., Yan, J., McGuire, M. A., Manley, M. E., Staunton, J. B., Hermann, R. P. & Frandsen, B. A. (2022). *Matter*, **5**, 1853–1864

Billinge, S. J. L. & Kanatzidis, M. G. (2004). *Chem. Commun.* pp. 749–760.

Billinge, S. J. L. & Levin, I. (2007). Science, 316, 561-565.

Bird, T. A., Herlihy, A. & Senn, M. S. (2021a). J. Appl. Cryst. 54, 1514–1520.

Bird, T. A., Wilkinson, M. G. L., Keen, D. A., Smith, R. I., Bristowe, N. C., Dove, M. T., Phillips, A. E. & Senn, M. S. (2021b). *Phys. Rev.* B, 104, 214102.

Campbell, B. J., Stokes, H. T., Tanner, D. E. & Hatch, D. M. (2006). J. Appl. Cryst. 39, 607–614.

Chepkemboi, C., Jorgensen, K., Sato, J. & Laurita, G. (2022). ACS Omega, 7, 14402–14411.

Coelho, A. A. (2018). J. Appl. Cryst. 51, 210-218.

Dagotto, E. (2005). Science, 309, 257-262.

Desgranges, L., Ma, Y., Garcia, P., Baldinozzi, G., Siméone, D. & Fischer, H. E. (2018). *Chem. Eur. J.* **24**, 2085–2088.

Di Salvo, F. J., Moncton, D. E. & Waszczak, J. V. (1976). Phys. Rev. B, 14, 4321–4328.

Dong, J., Wu, C.-F., Pei, J., Sun, F.-H., Pan, Y., Zhang, B.-P., Tang, H. & Li, J.-F. (2018). J. Mater. Chem. C, 6, 4265–4272.

Efrem D'Sa, J. B. C., Bhobe, P., Priolkar, K., Das, A., Paranjpe, S., Prabhu, R. & Sarode, P. (2005). J. Magn. Magn. Mater. 285, 267– 271

Egami, T. & Billinge, S. J. L. (2012). *Underneath the Bragg Peaks: Structural Analysis of Complex Materials*, 2nd ed. Amsterdam: Elsevier.

Fang, X.-Y., Hong, H., Chen, P. & Chiang, T.-C. (2017). Phys. Rev. B, 95, 201409.

Forse, A. C., Merlet, C., Allan, P. K., Humphreys, E. K., Griffin, J. M., Aslan, M., Zeiger, M., Presser, V., Gogotsi, Y. & Grey, C. P. (2015). *Chem. Mater.* 27, 6848–6857.

Frandsen, B. A. & Billinge, S. J. L. (2015). *Acta Cryst.* A**71**, 325–334.
Frandsen, B., Yang, X. & Billinge, S. J. L. (2014). *Acta Cryst.* A**70**, 3–11.

Gawryluk, D. J., Klein, Y. M., Shang, T., Sheptyakov, D., Keller, L., Casati, N., Lacorre, P., Fernández-Díaz, M. T., Rodríguez-Carvajal, J. & Medarde, M. (2019). *Phys. Rev. B*, **100**, 205137.

Herlihy, A., Bird, T. A., Ridley, C. J., Bull, C. L., Funnell, N. P. & Senn, M. S. (2022). *Phys. Rev. B*, **105**, 094114.

Juhás, P., Farrow, C., Yang, X., Knox, K. & Billinge, S. (2015). Acta Cryst. A71, 562–568.

Keen, D. A. (2020). Crystallogr. Rev. 26, 143-201.

Keen, D. A. & Goodwin, A. L. (2015). Nature, 521, 303-309.

Kerman, S., Campbell, B. J., Satyavarapu, K. K., Stokes, H. T., Perselli, F. & Evans, J. S. O. (2012). *Acta Cryst.* A68, 222–234.

Kriegner, D., Výborný, K., Olejník, K., Reichlová, H., Novák, V., Marti, X., Gazquez, J., Saidl, V., Němec, P., Volobuev, V. V., Springholz, G., Holý, V. & Jungwirth, T. (2016). *Nat. Commun.* 7, 11623.

Liu, H., Zhang, W., Halasyamani, P. S., Stokes, H. T., Campbell, B. J., Evans, J. S. O. & Evans, I. R. (2018). J. Am. Chem. Soc. 140, 13441– 13448

Manzeli, S., Ovchinnikov, D., Pasquier, D., Yazyev, O. V. & Kis, A. (2017). *Nat. Rev. Mater.* **2**, 17033.

McDonnell, M. T., Olds, D. P., Page, K. L., Neufeind, J. C., Tucker, M. G., Bilheux, J. C., Zhou, W. & Peterson, P. F. (2017). *Acta Cryst.* A**73**, a377.

Momma, K. & Izumi, F. (2011). J. Appl. Cryst. 44, 1272-1276.

- Moya, J. M., Huang, C.-L., Choe, J., Costin, G., Foster, M. S. & Morosan, E. (2019). *Phys. Rev. Mater.* **3**, 084005.
- Neuefeind, J., Feygenson, M., Carruth, J., Hoffmann, R. & Chipley, K. K. (2012). Nucl. Instrum. Methods Phys. Res. B, 287, 68–75.
- Prescher, C. & Prakapenka, V. B. (2015). *High Pressure Res.* **35**, 223–230.
- Ren, Y., Yang, J., Jiang, Q., Zhang, D., Zhou, Z., Li, X., Xin, J. & He, X. (2017). J. Mater. Chem. C, 5, 5076–5082.
- Stokes, H. T., Hatch, D. M. & Campbell, B. J. (2023). *ISODISTORT*. *ISOTROPY Software Suite*. https://stokes.byu.edu/iso/isotropy.php. Subedi, A. (2022). *Phys. Rev. Mater.* **6**, 014602.
- Toby, B. H. & Von Dreele, R. B. (2013). *J. Appl. Cryst.* **46**, 544–549. Tokura, Y., Kawasaki, M. & Nagaosa, N. (2017). *Nat. Phys.* **13**, 1056–1068

- Xu, Y., Li, W., Wang, C., Li, J., Chen, Z., Lin, S., Chen, Y. & Pei, Y. (2017). J. Mater. Chem. A, 5, 19143–19150.
- Yang, X., Juhás, P., Farrow, C. & Billinge, S. J. L. (2015). arXiv:1402.3163.
- Yin, X., Tang, C. S., Zheng, Y., Gao, J., Wu, J., Zhang, H., Chhowalla, M., Chen, W. & Wee, A. T. S. (2021). *Chem. Soc. Rev.* **50**, 10087– 10115
- Young, C. A. & Goodwin, A. L. (2011). J. Mater. Chem. 21, 6464–6476.
- Zheng, Y., Lu, T., Polash, M. M. H., Rasoulianboroujeni, M., Liu, N., Manley, M. E., Deng, Y., Sun, P. J., Chen, X. L., Hermann, R. P., Vashaee, D., Heremans, J. P. & Zhao, H. (2019). *Sci. Adv.* 5, eaat9461.
- Zhu, H., Huang, Y., Ren, J., Zhang, B., Ke, Y., Jen, A. K.-Y., Zhang, Q., Wang, X.-L. & Liu, Q. (2021). *Adv. Sci.* **8**, 2003534.